JOURNAL OF COMPUTATIONAL PHYSICS 55, 347–368 (1984)

Three Dimensional, Stratified Gas Flows Past an Obstacle

MARK A. HAUSMAN AND WILLIAM W. ROBERTS, JR.

Department of Applied Mathematics and Computer Science, University of Virginia, Charlottesville, Virginia 22903

Received August 2, 1983; revised November 15, 1983

An "N-body" computer code is developed to study supersonic gas flows in a rarefied, strongly stratified medium. Results of numerical simulations both with and without an obstacle obstructing the flow are presented, focusing upon three dimensional effects. In particular, the systematic gas motions and density perturbations induced by a flat plate whose normal vector is parallel to the direction of umperturbed flow and perpendicular to the stratification gradient are discussed. Such a plate can be regarded as a useful approximation to a scoop in a gas centrifuge.

I. INTRODUCTION

The interaction of a stratified gas impinging supersonically upon a solid body comparable in size to the gas scale height is a problem which has received virtually no theoretical attention until recently. The problem, difficult as it sounds, is made still more intractable if we further stipulate that the gas is sufficiently rarefied so that the collisional mean free path of its constituent molecules is similar to the stratification scale length. Traditional methods of computing gas properties all fail in this regime. If the mean free path were much *longer* than the other relevant length scales, we could treat the gas as if it were collisionless and calculate its properties from the mean trajectories of noninteracting molecules, whereas a dense gas might be treated by the traditional fluid-dynamical equations. In the situation under consideration, however, we must develop a computational method which takes into account both interactions between molecules and the smoothing effects induced by the long mean free path.

This problem has been little studied, of course, because there are few natural or artificial situations in which this combination of parameters occurs. For example, in the earth's atmosphere, the mean free path does not become comparable to the scale height until some 500 km above the ground, where both approach 100 km (Allen [1]) and the local one dimensional velocity dispersion ("sound speed") is roughly 1 km s^{-1}. Our hypothetical problem would then be equivalent to examining the "atmospheric" perturbations on an orbiting billboard approximately the size of Connecticut.

There is, however, one practical situation where these various length scales may converge. In a rapidly rotating gas centrifuge, the density scale height may be of

0021-9991/84 $3.00

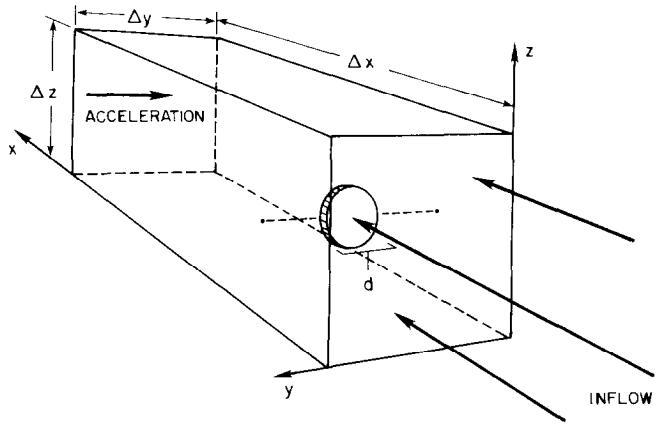

FIG. 1. Schematic diagram of the computational volume. Particles are injected at the $x = 0$ face. Acceleration is in the $-y$ direction. The plate reflects particles.

order 1 cm, while the mean free path, much shorter at the wall, may increase to centimeter scales near the center. If a solid object of similar size (e.g., a scoop) is introduced into the rotor and held fixed in the inertial frame, the hypothesized supersonic relative velocities may easily be achieved.

In the computer models to be described, we have inserted a flat circular plate (see Fig. 1), assumed to be a diffuse elastic scatterer, into a stratified, supersonic gas whose scale height and mean free path (at the level of the plate's center) are both comparable to the plate diameter. We orient the plate so that its normal vector is in a plane of constant (unperturbed) density (i.e., perpendicular to the stratification gradient, hereafter called the y or "radial" direction), and parallel to the free-stream (unperturbed) flow (hereafter called the x or "circumferential" direction). In this way we may examine the complicating effects introduced by the combination of intermediate mean free path and short scale height: if the gas were purely collisionless, regardless of the scale height, the plate would reflect impingent particles back upstream and reduce or leave unaltered the gas density at all points downstream; while an unstratified (long scale height) gas, regardless of its mean free path, would show reflection symmetry across the x–z plane which includes the plate's center [e.g., $\rho(x, y_0 + \Delta y, z) = \rho(x, y_0 - \Delta y, z)$ for all $x, \Delta y, z$].

In the following section we briefly describe the N-body, Monte Carlo technique which was developed for these calculations. We next describe the results of several simulations, comparing three dimensional effects induced by an obstructing plate to the "null" results of unobstructed flow calculations. We conclude with a discussion of the major features and limitations of our models and suggestions for further study.

II. Computational Technique

A. *Monte Carlo Particle Dynamics*

The classical equations of gas dynamics implicitly assume that the bulk fluid properties within any infinitesimal volume element depend only on the average behavior of its constituent molecules and the properties of adjacent elements. Long collisional mean free paths introduce nonlocal effects into the fluid picture, because each volume element may be influenced by all other elements whose distance is less than a few mean free paths.

When we model systems whose significant dimensions are comparable to the mean free path, we may not employ the continuum Navier–Stokes equations. Instead, we compute the trajectories of individual particles, each of which is assumed to be "representative" of some (large) number N of real gas molecules. These particles will move at typical velocities, be subject to the same external forces, and reflect from the same solid boundaries as do real molecules, and will collide with one another sufficiently frequently that the collision rate per particle is the same as the rate expected per molecule. (This last condition makes the technique impracticably time consuming for computing any but rather long mean free path, low collision rate models.) The gas density and velocity distribution near any point are estimated from the number and velocities of computer particles found within a small volume element surrounding the point.

The collision frequency per gas molecule ν is related to the local number density n and average relative velocity $\bar{v}_r$ by the relation

$$\nu = n\sigma\bar{v}_r \equiv \bar{v}_r/(\sqrt{2}\,\lambda), \tag{1}$$

where σ is the collisional cross section and λ the mean free path. Thus, if our computer particles are to have the same collision rate, they must have the same mean free path (and relative velocity). Since the number density of computer particles is a factor N below that of real particles, the "effective" cross section Σ must be proportionately larger:

$$\Sigma \equiv \sigma n_{\text{mol}}/n_{\text{part}} = N\sigma. \tag{2}$$

A straightforward computational method would be to follow the exact trajectories of all particles and calculate an interaction whenever a pair is found to come within a collision diameter of each other. However, this requires knowledge of the distance between all pairs of particles, and since computation time then increases with the square of the number of particles, high-precision computations would be hopelessly time consuming. Instead, we use a probabilistic, Monte Carlo method of collision calculations.

In this technique (adopted from Bird [2, 3]), the trajectories of individual particles are followed exactly, but not the separation of pairs. Instead, at the end of each time step, pairs of particles within each (small) volume element (or "cell") are randomly

chosen to collide, without regard to their spatial separation. The rationale for this is the near uniformity of the density and velocity field within a sufficiently small volume element, so that each particle represents N real molecules *spread throughout* the cell, and a pair of representative molecules may as easily be close together as distant. To ensure that this assumed, near uniformity obtains, it is highly desirable that the cell sizes be less than the mean free path. (This may not always be practicable in a highly stratified gas, whose λ may vary by orders of magnitude.)

Two particles in a cell are chosen at random; comparison of their relative velocity to a random number determines whether the pair is accepted as a "collision" (since molecular collision rate goes up with relative velocity, the probability of acceptance must be proportional to v_r). The postcollision velocities of the pair are altered appropriately. For the models to be described, we have assumed elastic, rigid-sphere collisions, so that the pair's relative velocity vector is *randomly* (and isotropically) scattered, while its magnitude remains unchanged. After the collision, a quantity of magnitude $2V/[k(k-1)\,v_r\Sigma]$ is added to a "time counter" for the cell in question, where k is the total number of computer particles in the volume V and v_r is the pair's relative velocity. Collisions are recorded within each cell until its time counter reaches the value of the integration time step Δt. Thus, the total number of collisions in a cell in one time step is roughly

$$N_{\text{coll}}(\Delta t) = k(k-1)\,\Sigma \Delta t \bar{v}_r/(2V). \tag{3}$$

The collision frequency per particle (recalling that each collision affects two particles) is then given by $\Sigma k \bar{v}_r/V$, which, as Eq. (2) shows, is equal to the molecular collision rate given by Eq. (1).

We allow particles to participate in more than one collision per time step. As multiple collisions may introduce a bias into the model it is desirable to keep our computational time step less than a typical collision time, if possible.

Our procedures need to be refined if the molecular density in the system to be modeled is very nonuniform, as would be the case in a stratified gas. If we were to use the same constant N to relate real molecules to computer particles everywhere in our system, the number of particles would either be too great for practical computation in dense regions or too small for reasonable statistics in rarefied regions, if not both. For a stratified gas, whose equilibrium, unperturbed density distribution is known, we can instead alter the proportionality constant N_i so that the number of particles is roughly the *same* in each cell i (N_i would then be proportional to the calculated equilibrium density). Note that the particle cross section Σ_i would vary from cell to cell (Eq. (2)).

The most important subtlety required by this refinement involves particles which move from one cell to another. When a particle representing N_i molecules crosses into a region where each particle represents N_j molecules, new particles may need to be created (if $N_i > N_j$) or the particle itself may need to be destroyed (if $N_i < N_j$). The exact prescription is chosen by comparing the remainder of (N_i/N_j) to a random number between zero and one; if the random number is greater than the remainder,

the particle becomes $\text{Int}(N_i/N_j)$ particles in cell j (note that if $N_i < N_j$, this requires us to "destroy" the particle), while a smaller random number converts the particle from cell i to $\text{Int}(N_i/N_j) + 1$ particles in j. If this necessitates the creation of new particles, they are given the same position and velocity perpendicular to the i–j border as the original particle, and the other two velocity components are chosen randomly from the velocity distribution appropriate for cell i. This prescription ensures the correct mass and perpendicular momentum flux across the cell border on average and a reasonable estimate of the transverse momentum flux (cf. Carter and Cashwell [4]).

A more accurate representation of the transverse momentum flux would be obtained if newly created molecules had precisely the same velocity components as the original molecule. However, the two or more identical particles would give a misleadingly high statistical weight to that velocity and lead to an artificially low estimate of velocity dispersion in the new cell. This problem becomes worse as N_i/N_j increases. A possibly useful compromise between preserving average flux and realistic dispersions would be to give each new particle the velocity of the original, perturbed by a normally distributed random number with standard deviation given by the velocity dispersion of cell i. Calculations using this prescription are currently in progress.

B. *A Stratified Gas Flow Model*

The computational volume of our models is a rectangular box of length 600 units (the x direction) and height and width both 200 units (see Fig. 1). (Because the significant physical scales are defined in terms of scale heights and mean free paths, and velocity in terms of gas sound speed, all of which may vary in actual physical problems, we choose arbitrary units for both size and speed, and hence, time.) The gas is injected at the $x = 0$ face with a one-dimensional velocity dispersion of 5 units and average speed of 20 to 30 units (Mach 4 to 6). A constant acceleration is imposed in the $-y$ ("outward") direction, whose magnitude is given by the formula

$$g = v_x^2/r = (Mv_d)^2/r, \tag{4}$$

where v_x and v_d are, respectively, the average free-stream (x) velocity and one dimensional velocity dispersion, M is the corresponding Mach number (v_x/v_d), and r an adjustable parameter representing the distance of the computation region from a hypothetical center of rotation. For most of the simulations to be described, r was chosen to be 800 units. The density scale height H of the gas, defined by the relation

$$n(y) = n(y_0)\exp[-(y - y_0)/H], \tag{5}$$

is then given by

$$H = v_d^2/g = r/M^2, \tag{6}$$

varying from 50 to 22 units as M varies from 4 to 6.

Since the collisional mean free path is inversely proportional to density [Eq. (1)], which falls exponentially with increasing y [Eq. (5)], we see that λ must *increase* exponentially with the same scale height H. We will model a system where λ_0 at the *midplane* of y ($y = 100$ units, hereafter called y_0) is 20 units long. We divide our box up into 24 slices in x, 5 in z (the "axial" direction), and 8 or 9 levels in y. For the purposes of defining y-dependent collisional cross sections for the particles (see above), we have assumed that the density of an equilibrium unperturbed flow will fall off with radius y as given by Eq. (5) and that a uniform number of computer particles will be followed in each y level, so that the local *particle* cross section Σ_i in cell i must be given [see Eqs. (1), (2), (5)] by

$$\Sigma_i = \Sigma(y_0) \exp[-(y_i - y_0)/H] = V/(\sqrt{2}\, k' \lambda_0) \exp[-(y_i - y_0)/H], \tag{7}$$

where k' is the number of particles required in a cell of volume V at level y_0 to give the "standard" mean free path λ_0 (=20). Note that if the *actual* particle density varies above or below the unperturbed, ideal value, the cross sections remain unchanged in each cell, so that the actual collision rate and mean free path will vary appropriately.

Particles are injected into the model at the $x = 0$ face and followed until they leave it again. The input rate is chosen so that, if the only "open" face through which particles are lost is the $x = 600$ face, the total number of particles in the (unperturbed) box would be 12,000. However, because it is at present impossible to model the entire interior of a gas centrifuge or other highly stratified system, we must resort to somewhat artificial boundary conditions. For most of the calculations to be described, we make *all* faces open ("vacuum" boundaries) except for the $y = 0$ plane (this must be reflecting, or the constant $-y$ acceleration will quickly empty the box of particles. Because the $y = 0$ plane specularly reflects particle velocities, it acts as an artificial plane of symmetry and may introduce nonphysical effects into the calculation. This is discussed further in Sections III.E and IV.). Thus, we will find that the average density towards high x ("downstream") is lower than realistic, as particles leaking out the $y = 200$ and $z = \pm 100$ faces are not replaced by particles coming in from outside. Because particles are introduced at high Mach number, though, we expect that the density of those which reach the downstream face will be a significant fraction of the density that a correctly modeled system would have. In order to calibrate the simulations of perturbed flows, we have run a few simulations in which particles are allowed to flow *unobstructed* through this "leaky tube"; the results will be described in the following section. We have also experimented by making *all* the faces (except the $x = 0$ and $x = 600$ planes) specularly reflective, so that no leakage occurs. In a real gas, of course, the boundary effects would be determined by physical conditions far from our small, selected volume (e.g., at a certrifuge's wall), and these cannot be anticipated for our models. We may reasonably hope, nonetheless, that our two kinds of artificial conditions (vacuum and reflective boundaries) may bracket the expected behavior.

Within this gas flow we place a circular plate of diameter 50 units. It is assumed to be a diffuse elastic scatterer; that is, particles which strike it are reflected in a

randomly chosen direction with unchanged velocity magnitude. The plate's normal vector is pointed towards the direction $(-1, 0, 0)$ so that it is perpendicular to the incoming flow. The center of the plate is at $(x_0, y_0, z_0) = (200, 100, 0)$, one third of the way down the central streamline, midway between the y and z faces, where the unperturbed mean free path should be 20 units.

The simulations were all performed in Cartesian coordinates, with constant H, g, and free stream v_x. If the acceleration were a centrifugal effect due to rotation, each of these quantities would vary with radial distance y while the direction of acceleration would vary with circumferential location x. As long as the height of the model volume (200 units) is much smaller than the mean radius ($r = 800$ units), we anticipate little effect upon our qualitative results. Because particles in low density regions of real centrifuges travel along straight paths of approximate length λ rather than circular orbits, our assumed constant, centrifugal acceleration [Eq. (4)] is valid only where $\lambda \ll r$. This is true for most of our computational region, but prevents our extending the Cartesian approximation much farther inward. Of perhaps greater significance is the fact that "centrifugal force" is velocity dependent, not constant for all particles. To examine this effect, we have computed a number of models in which the acceleration magnitude is proportional to v_x^2 for each particle. The results were found to be qualitatively similar to constant-acceleration models, so we feel justified in applying our constant-g results to rotating systems.

As stated above, our results should be applicable to *any* system with the stated ratios of scale height and mean free path to obstacle size and streaming velocity to sound speed. Consequently, we have left the dimensional quantities in arbitrary units.

III. Results

A. *Calibration Model: No Obstacle*

In order to estimate the inaccuracies introduced into our computations by the vacuum boundary conditions, we have run several simulations with no plate. Particles are injected at the $x = 0$ face with average $v_x = 20$ units (Mach 4) and followed until they left the far end or any of the open sides. In a true, constant-acceleration equilibrium, we would expect no deviation from the mean input velocity $(v_x, 0, 0)$ with position, and a uniform density of computer particles [i.e., molecular density falling exponentially, with scale height given by Eq. (6)].

Figure 2 shows the resulting mean velocity fields for Case 1, a Mach 4 run ($H = 50$ units). Each velocity point represents the average of some 50 determinations of the mean velocity for the appropriate cell, the individual determinations taken at intervals of 10 time units (one third the time required for an average particle to travel the length of the tube). Estimated random errors for each point are in the range 0.2 to 0.4 unit.

Figure 2a shows the deviation of v_x from its input value as a function of x location, for different y levels, in the z slice $-20 < z < 20$. We see a slow, monotonic rise to

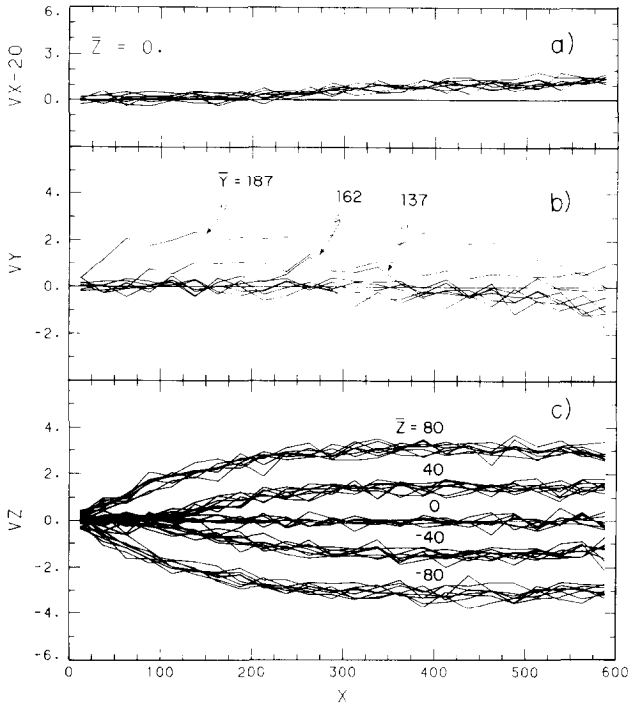

FIG. 2. Velocity fields for Case 1 ($M = 4$, $v_d = 5$, $H = 50$, and no obstacle): (a) deviations of v_x from 20 in the slice $-20 < z < 20$, for all y levels. (b) v_y in the slice $-20 < z < 20$, for all y levels. (c) v_z, for all y levels and z slices. The five clumps, from top to bottom, represent $\bar{z} = 80$, 40, 0, -40, -80.

about 1.5 units as x (= travel time), increases, suggesting that slower particles are preferentially scattered out of the computational volume (their collision rate is similar, but it requires more time, therefore more chances for collisions, before they traverse the box). The effect clearly does not depend significantly on y. Equivalent figures for different z slices are virtually indistinguishable, indicating no z dependence, either.

Figure 2b shows a plot of v_y versus x for all y levels in the same z slice. The outermost levels (low y value, near the reflecting boundary) show no significant deviation from zero. However, the innermost two y levels have significantly positive velocity. Particles there may move inward from the outer layers (i.e., towards increasing y), but there are no particles past the inner vacuum boundary to move outward; thus, these layers show a net inward flux. There is little x variation beyond the first few x slices, and the other z slices are found to exhibit similar behavior.

Figure 2c shows the variation of v_z with x. Each cluster of curves represents the various y levels in a single z slice, whose centers, from top cluster to bottom, are at $\bar{z} = 80$, 40, 0, -40, and -80. We see that v_z is roughly proportional to z position, again representing the leakage of particles out of the box. There is no significant y dependence.

Figure 3 shows contours of equal *particle* densities for this run projected against the x–y axis. A correctly represented system would, of course, show uniform density. The contours represent linearly spaced isodensity levels varying from 12 at the left (low x) to 4 in the upper right (high x, high y). We see, then, that the boundary conditions we have chosen allow our "uperturbed' density to fall by a factor of 3 from one end of the box to the other. Note that because we have plotted particle density, the exponentially varying ratio of particle to gas molecule number has been factored out. A contour plot of *gas* isodensity would show nearly horizontal stratification, the particle loss apparent only as a slight "tipping" of the contours towards the lower right.

Figures 2 and 3 indicate that the effects of the artificial boundary conditions, while far from negligible, are nevertheless orderly and predictable. As long as our simulations *with* obstacles are at similarly high Mach numbers, we should be able to separate the effects of the modeled perturbation from those of the vacuum boundaries.

A similar, no-obstacle simulation has been carried out with a Mach 6 gas (Case 4, $H = 22$ units). The deviations of both density and velocity from position-independence were comparable, but the maximum v_x deviation was reduced (to about 0.8) and the density at high x was slightly more than half that at the low x end. This confirms our supposition that higher Mach number simulations show reduced leakage effects. A third run (Case 6), with Mach 4 but $H = 25$, showed results very similar to those of Case 1.

B. *Plate* $M = 4$

Case 2 represents a Mach 4 model ($H = 50$ units) in which a 50-unit diameter plate is inserted perpendicular to the incoming flow, 200 units downstream of the $x = 0$ boundary. Figure 4 shows the velocity field in the central ($-20 < z < 20$) slice, which contains the plate center. Figure 4a shows the sudden dip in v_x which the obstacle produces in the central y layers. Downstream of the obstacle v_x approaches its unperturbed (Case 1) value. The z symmetry of our system results in no net z motion in this central slice. However, v_y in the innermost y levels of this slice (Fig. 4b) is considerably enhanced over that in Case 1, especially between 50 units upstream and

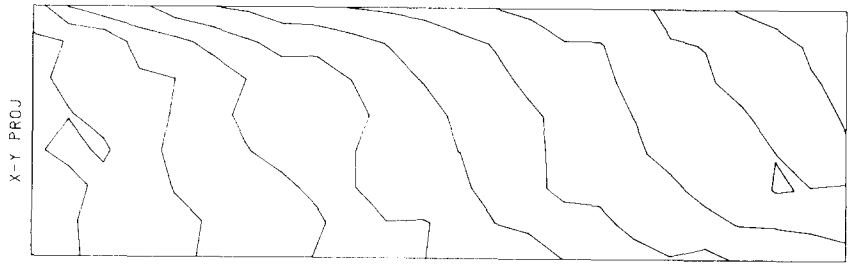

FIG. 3. Contour plot of particle surface density, projected onto the x–y plane. y increases upward, x to the right. The contour levels are linear, separated by one (arbitrary) density unit, and decline from 12 at left to 4 at upper right.

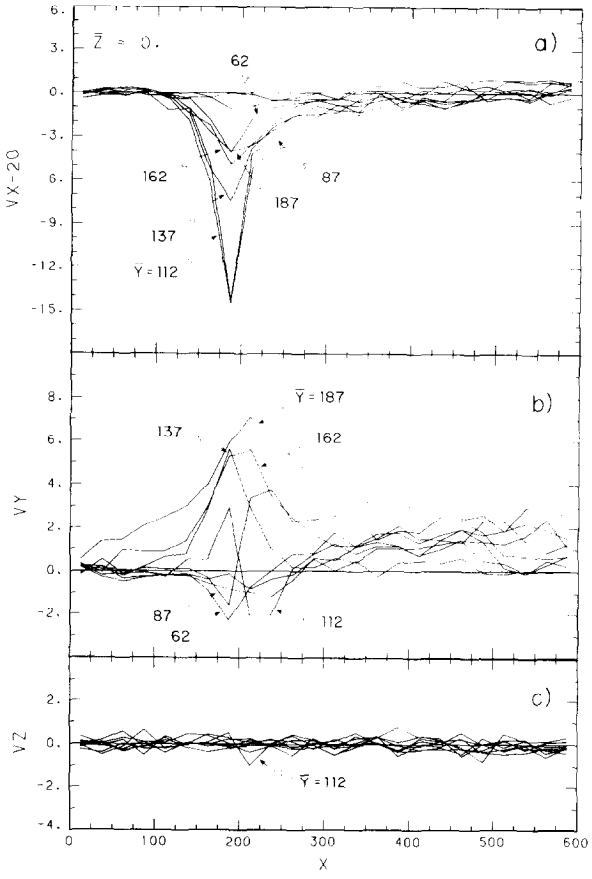

FIG. 4. Velocity fields for Case 2 ($M = 4$, $v_d = 5$, $H = 50$, and plate in), for all y levels in the slice $-20 < z < 20$. (a) Deviations of v_x from 20, (b) v_y, (c) v_z.

100 downstream of the plate. The downstream enhancement is a collisional effect, due to the scattering produced when the deflected stream interacts with the incoming stream.

Figure 5 shows the situation in the uppermost ($60 < z < 100$) layer. The v_x and v_z velocities show dips and peaks, respectively, but of low amplitude and spread over a broader Δx, Δy region than the v_x dip near the plate. The inner-layer v_y enhancement is only slightly reduced from that in Fig. 4b. The position of maximum perturbation is shifted downstream of the plate for each velocity. We see that the perturbed velocity in the (inner y, upper z, middle x) cells of this model is directed more nearly in the $+y$ than the $+z$ direction.

The velocity fields in the ($20 < z < 60$) slice are intermediate between those shown in Figs. 4 and 5. Both velocity fields and density distributions below the plate ($z < 0$) are, within stochastic errors, z reflections of those above.

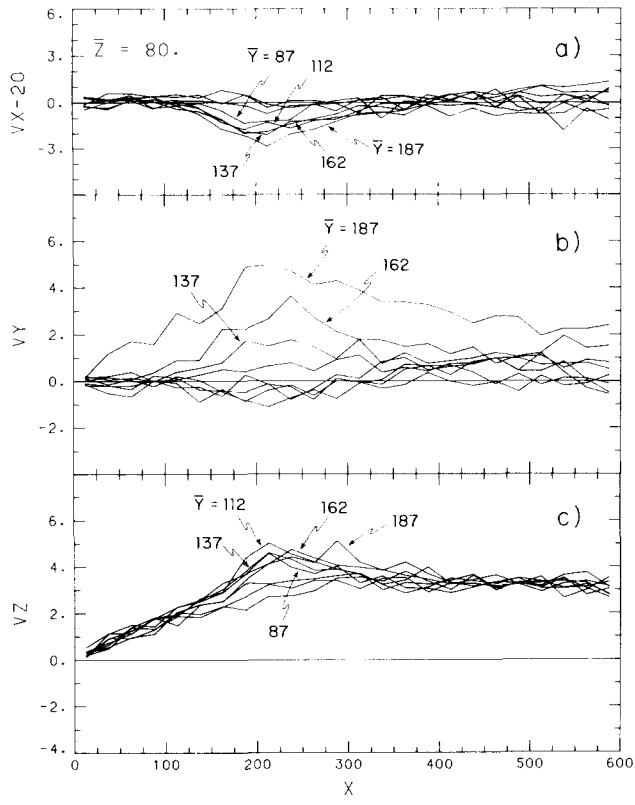

FIG. 5. Velocity fields for Case 2, for all y levels in the slice $60 < z < 100$. (a) $v_x - 20$, (b) v_y, (c) v_z.

Figure 6 shows the particle density contours projected against the x–y plane for three z slices centered on the values (from top) $z = 80$, 40, 0. At the plate level ($z = 0$), there is a strong compression where the incoming stream strikes (this would be a strong shock if λ were much shorter) and a low density region behind the plate. The isoparticle contours spread out behind the shock almost symmetrically around $y = y_0$. However, as we move upwards the density perturbation becomes far less symmetrical: a ridge of increased density moves preferentially inward (high y) from the plate level in the $z = 40$ level. This effect is a result of the short scale height of the

contours show horizontal stratification as the principle effect. Figure 7 is the *gas* isodensity plot for Case 2 in the central ($z = 0$) slice. Only immediately before and behind the plate is the density perturbation sufficient to "break" the stratification. Elsewhere (and in other z levels) the perturbation only shows itself as alterations in

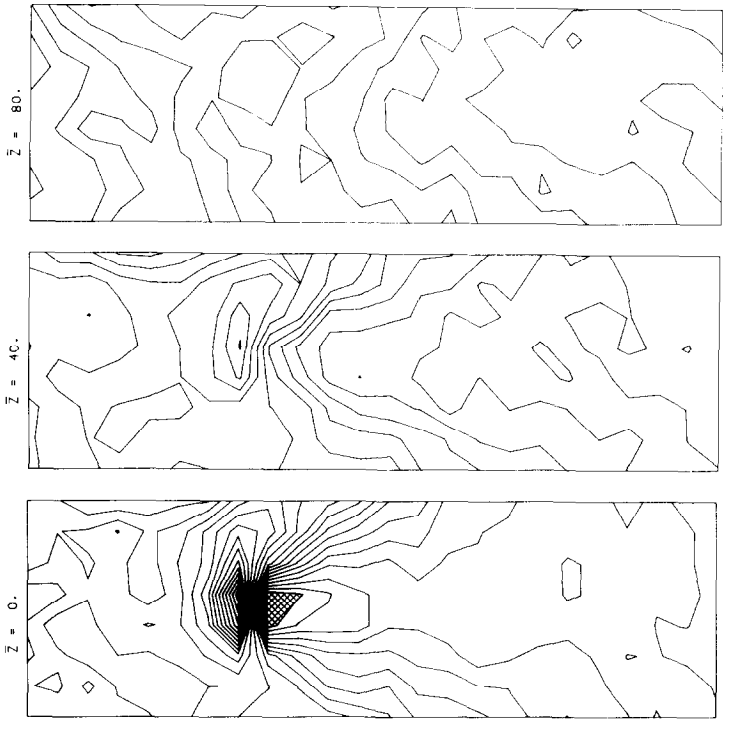

FIG. 6. Particle-density contours for Case 2. Contour levels are linear and separated by 1 unit. From top, slices are those centered at $z = 80$, 40, 0. Hatched regions represent local minima. Density decreases to the right, in general.

the slope or crowding of the stratification contours. We see, then, that locally significant density changes may have only minor effect on large-scale appearance, yet still considerably alter the velocity field (Figs. 4, 5).

C. *Plate*, $M = 6$

Case 3 represents a model similar to Case 2, but with a Mach number of 6 ($H = 22$ units). The $z = 0$ level shows tremendous velocity fluctuation (Fig. 8). The v_x

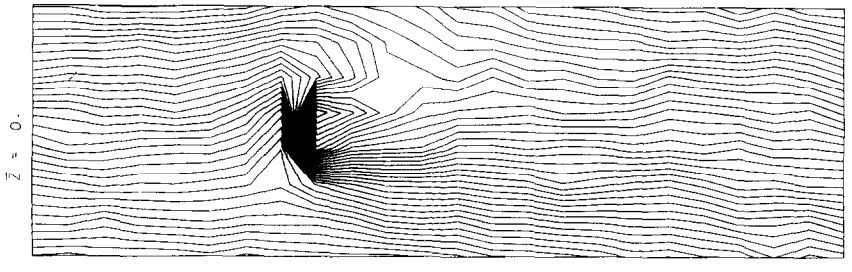

FIG. 7. *Molecule-density* contours for Case 2, in slice $-20 < z < 20$ (contains plate center). Contour levels are *logarithmic*, separated by Dex(0.05). Maximum density is at bottom ($y = 0$).

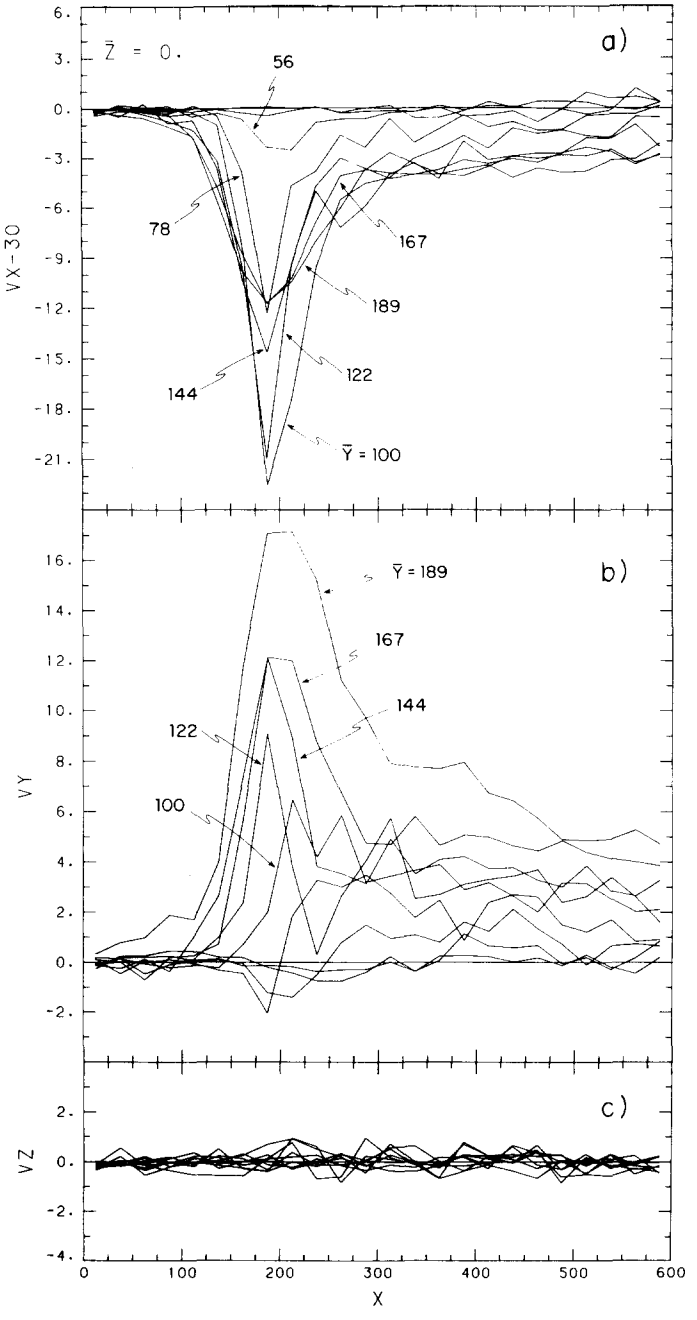

FIG. 8. Velocity fields for Case 3 ($M = 6$, $v_d = 5$, $H = 22$, and plate in) for all y levels in the slice $20 < z < 20$. (a) $v_x - 30$; (b) v_y; (c) v_z.

curves show the same sharp dips as does Fig. 4, but with still greater amplitudes (in fact, the perturbation amplitudes are about the same fractions of the undisturbed, free-stream velocities in both Cases 2 and 3). However, v_x hovers below zero far downstream, particularly in the innermost cells. Meanwhile, v_y (Fig. 8b) shows quite strong inward motion in all but the outermost cells. As usual, the z reflection symmetry prevents any net v_z motion in this level.

In the uppermost z slice (Fig. 9), the velocity field shows much the same trend that we saw in Case 2, again with increased perturbation amplitude. Here, too, the v_x perturbations show reduced amplitude, broader spatial extent, and downstream shifting of their peaks compared to the central z slice. Notice that v_x does not return to its unperturbed value in the innermost y levels. Figure 9b shows the strong inward expansion exhibited by v_y. As was true for Case 2, the peculiar velocity in the (high y, high z, middle x) cells is primarily inward rather than upward, but Fig. 9c shows a fairly strong perturbation even in v_z.

Figure 10 shows the particle isodensity contours for the same three z slices as Fig. 6. Here the effects of the plate may be seen even in the uppermost ($z = 80$) level, in the form of a high (relative) density region near the innermost surface. At the plate ($z = 0$), the contours do not show the y symmetry apparent for Case 2; instead the (particle) density is markedly greater at high than low y. In the $z = 40$ level, the y asymmetry is still more marked, with a high density ridge pointing towards high x and y and a low density region displaced outward of the plate center.

Remarkably, the *molecular* isodensity contours for Case 3 show *less*, rather than more, small scale detail than do those for Case 2. This is a consequence of Case 3's reduced scale height, so that on large scales the exponential falloff disguises the local density perturbations, which nonetheless quite significantly alter the velocity field.

D. *Short Scale Height*, $M = 4$

Case 5, which has a Mach number 4 but scale height of only 25 units, is designed to determine whether the differences between Cases 2 and 3 are primarily due to the different speeds or different scale heights. Remarkably, almost all of Case 5's results were extremely similar to either Case 2 or Case 3.

The v_x perturbation is intermediate between that in Cases 2 and 3, showing fairly high amplitude dips which extend across several y levels but return near to zero downstream, as is true for Case 2's inner levels (but not Case 3). The z velocity resembles that in Case 2 for all z slices while v_y resembles that in Case 2 except for a slightly increased amplitude. On the other hand, the particle density contours are very similar to those of Case 3: a strong, high density ridge extends to a high (relative) density region at the innermost border, while a rarefied region appears downstream and slightly outward of the plate center.

This gratifying separation of effects allows us to distinguish their principal causes. While the form of the perturbed velocity is most strongly influenced by the incoming speed, the density perturbations are strongly affected by the magnitude of the scale height.

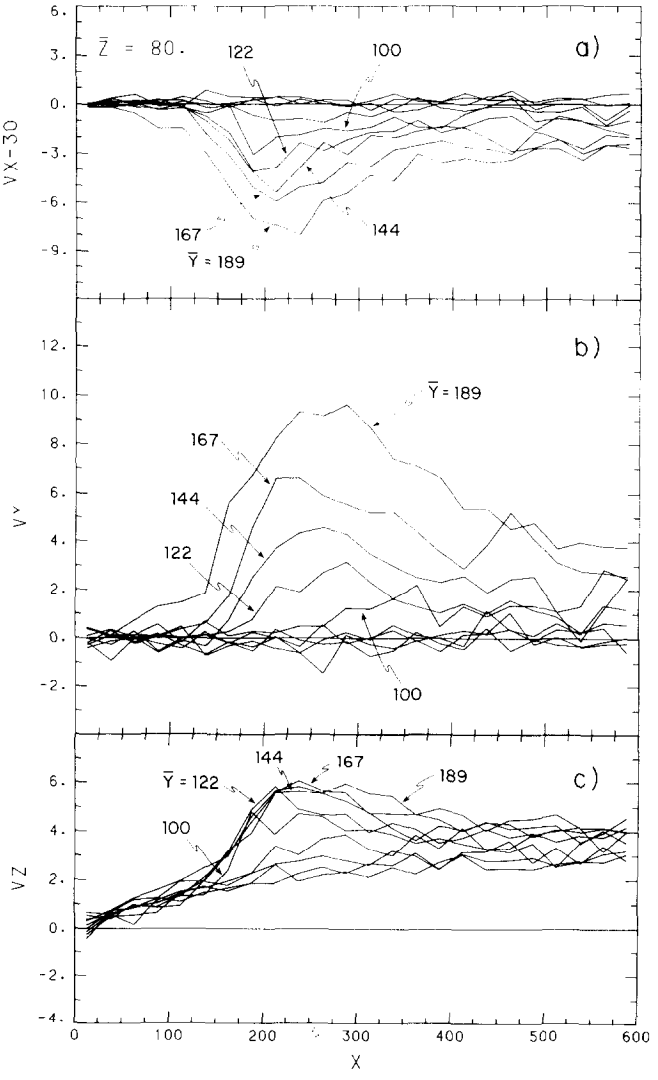

FIG. 9. Velocity fields for Case 3 for all y levels in the slice $60 < z < 100$. (a) $v_x - 30$, (b) v_y, (c) v_z.

E. *Reflecting Tube*, $M = 4$

In an effort to determine how strongly the foregoing results may be influenced by the vacuum boundary condition, we consider one further case, T1. This is similar in all respects to Case 2 ($H = 50$, $M = 4$), except that all of the y and z boundaries are specularly reflecting. Since particles may move in or out only through the $x = 0$ and $x = 600$ faces, we nearly eliminate any leakage effect, although the boundary reflections introduce unphysical effects of their own.

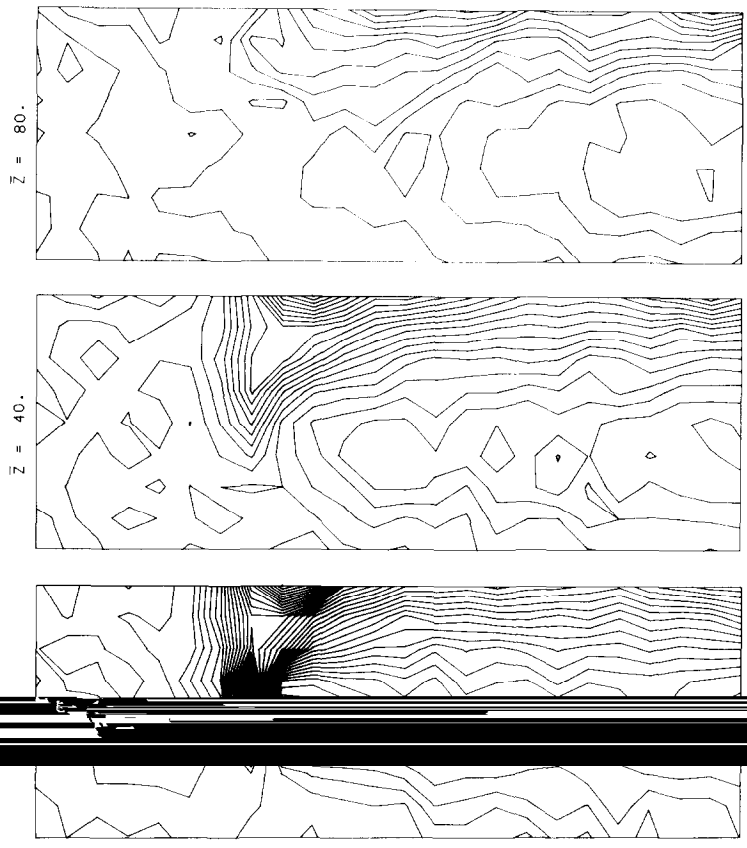

FIG. 10. Particle density contours for Case 3. Contour levels are linear and separated by 1 unit. From the top, slices are centered at $\bar{z} = 80, 40, 0$.

The results are very similar to Case 2. In contrast to the nonzero velocity fields due to leakage in Case 1 (Fig. 2), the *unperturbed* fields in a reflecting tube should be zero (as indeed they are far upstream and downstream of the plate). The perturbed fields in Case T1 ($150 < x < 300$) are just about what one would get by subtracting the curves of Fig. 2 from those of Figs. 4 and 5: bulges or dips of greater or lesser amplitude and width, gradually approaching the unperturbed value (i.e., zero) far downstream. The principal systematic difference is that v_y in the innermost y levels remains close to zero. This is a consequence of inward-moving particles being reflected back outwards at the wall.

The density contours of Case T1 are also qualitatively similar to those of Case 2 (Fig. 6), showing a moderate density ridge stretching towards high y and x and a rarefied region almost centered at y_0. The only significant differences, the higher overall density downstream and particularly at the inner y boundary, are obvious results of the reduced leakage. In general, the gratifying similarity of Cases 2 and T1

leads us to believe that, despite the uncertainties of the boundary conditions, we may make qualitative predictions about the behavior of a stratified, rarefied, supersonic gas.

F. *Specularly Reflecting Plate*, $M = 4$

Case S1 is designed to test the effects that our plate's reflection properties have on the gas flow. In this case, particles impinging upon the plate are reflected *specularly*, i.e., their x velocities are reversed while their y and z velocities remain unchanged, in contrast to the isotropic scattering displayed by our other models. In all other respects, Case S1 resembles Case 2, with open boundaries (except at $y = 0$), $M = 4$, and scale height $H = 50$.

Remarkably, the velocity fields in Case S1 have *no* statistically significant differences from those in Case 2 (Figs. 4, 5), possibly excepting a marginally deeper preplate dip in v_x (cf. Fig. 4a) and slightly greater v_y and v_z expansions far from the plate axis (cf. Figs. 5b and 5c). The particle densities are just as similar, Case S1's contour diagrams being essentially indistinguishable from Fig. 6.

The surprising similarity of results for this specular reflector to the diffuse scatterers of our other models can be understood when we examine the dispersions in the x, y, and z velocities. It turns out that the molecular mean free path immediately in front of the plate is sufficiently short (the local threefold increase over average particle density reduces λ near the plate axis to about 7 units) that the velocity dispersions are nearly isotropized within one cell-width of the plate. Thus the actual direction of the postscattering particles matters little, as long as the velocity magnitude remains the same, for they will immediately collide with incoming particles and scatter elastically and isotropically. This may no longer be true if the plate were a *cold* diffuse scatterer, so that impinging molecules lose velocity (and kinetic energy) in the reflection process.

IV. Discussion

The simulations we have described, modeling the supersonic interaction of a rarefied, stratified gas with a flat "scoop" comparable in size to the gas scale height and mean free path, show qualitatively similar results despite the differences in Mach number, scale height, boundary conditions, and reflection law chosen. At the z level of the plate, an enhanced-density ridge forms in front of the plate and stretches downstream and inward from it, while a reduced-density region appears downstream and, in short scale-height flows, slightly outward of the plate location. These effects weaken as we move axially away from the plate, lingering longest as a density enhancement in the innermost (high y) levels. The circumferential velocity shows sharp dips immediately in front of the plate, which broaden, decline in amplitude, and shift downstream with increasing (axial) distance from it. The radial velocity shows a broad but strong inward motion at the plate level and in the innermost cells modeled,

which gets progressively weaker above and below plate level, while the axial velocity shows a symmetrical, subsonic expansion away from the plate center.

The complicated nature of this gas flow, quite apart from its details, indicates that short scale height systems interacting with finite-sized solids cannot be effectively modeled in detail by two dimensional calculations. Figures 6 and 10 demonstrate how the density varies independently in all directions and shows no simplifying symmetries which might allow the problem to be recast into two dimensions.

Perhaps the most obvious "three-dimensional" effect of the interaction of short scale heights with intermediate mean free paths is the net inward motion of the scattered gas (whose initial, postscattering velocity is symmetric around the plate axis). We have seen that in regions inward of the plate, the velocity is more nearly radial than axial (Figs. 5 and 9). The inward motion persists even in Case T1, so it is not purely an artifact of the open boundary at $y = 200$ in the other models. However, due to the nearly-exponential density law, these regions have far smaller molecular density than the cells near y_0 in which velocity is more nearly axial. Figure 11 demonstrates a "macroscopic" measure of the importance of the radial motion. The mass flux through the innermost y boundary for Case 2 (Fig. 11a) shows a strong bulge just downstream of the plate location ($x_0 = 200$) compared to the unobstructed (Case 1) flow; the maximum difference is about 1.3 flux units, declining far downstream. Figure 11b shows a similar comparison for mass flux through the top z boundary. Here the deflected flow reaches a maximum difference from the no-obstacle flow at about the same x value, but the difference is closer to 2.6 in the *same* mass flux units. Hence, the radial expansion revealed in these calculations, though locally strong, apparently plays only a secondary role in establishing global conditions. (Note that both boundaries considered in Fig. 11 were the same distance—100 units—from the plate center; boundaries at other distances would no doubt show different values.) The differential mass flux plots of the other obstacle/no obstacle pairs studied (Cases 3 and 4, Cases 5 and 6, Case T1 and a no-obstacle, $M = 4$ reflecting tube) showed very similar behavior to that in Fig. 11, even to the approximate magnitudes of the flux differences.

We have predicted a number of general effects that obstructed flow in a centrifuge might produce. Are these predictions subject to experimental test? The local density perturbations shown in Figs. 6 and 10 might in fact be very difficult to map in a real system; Fig. 7 demonstrates that the exponential dependence will effectively mask all but the strongest perturbations, unless extremely accurate positioning is available. The velocity fields hold out more hope, however. In particular, the radial motion of the inward gas and the radial mass flux shown in Fig. 11 are important model results for which unambiguous tests should be possible. Moreover, the effects of a somewhat larger plate (compared to either scale height or centrifuge diameter) would be expected to enhance the density perturbations (cf. Sect. III.D).

We believe that the Monte Carlo particle dynamics computational algorithm described in Section II and used for our simulations is a good choice for modeling the intermediate-λ regime of interest here. The main problems arising from its use are spatial resolution and computer time requirements. The computational cells used to

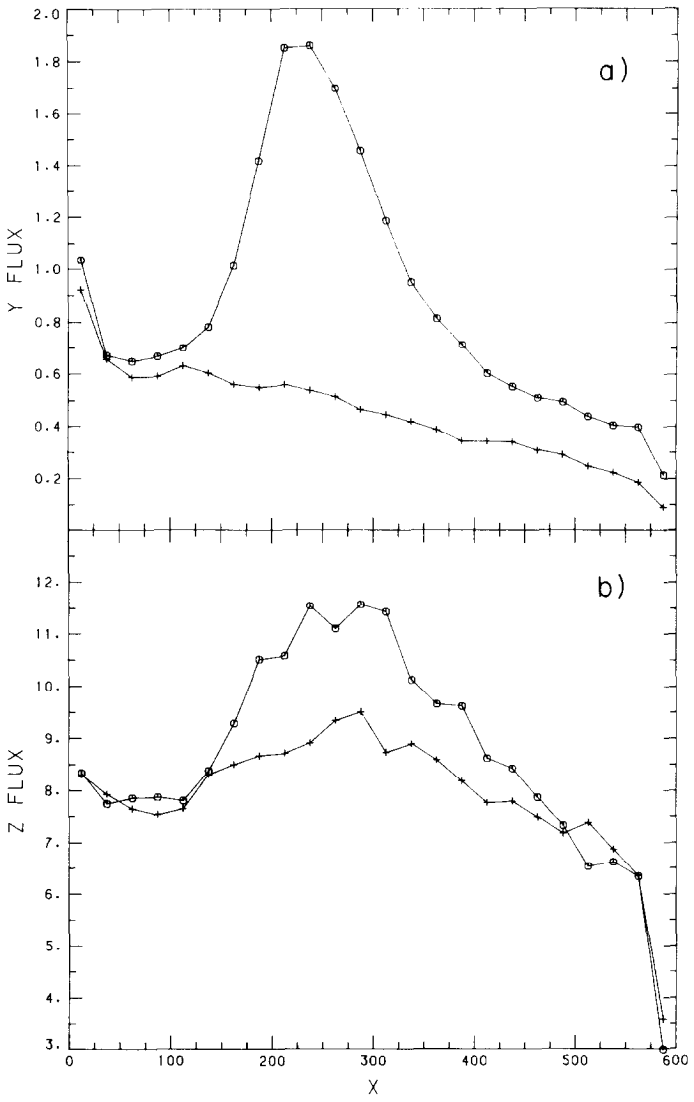

FIG. 11. Mass fluxes through boundaries of Case 1 (crosses) and Case 2 (circles). Flux units are arbitrary, but the same for each curve. (a) Flux through $y = 200$ boundary (each point is a summation over all z slices at that x). (b) Flux through $z = 100$ boundary (each point is a summation over all y slices at that x).

predict particle collision rates, local density, and velocity fields are of size $25 \times 25 \times 40$ units (x, y, z dimensions), not much smaller than the plate itself. In a short-λ gas this would give ample reason to fear that we are washing out small-scale structure and smoothing out shocks. However, we have seen (Figs. 6, 10) that most of the interesting small-scale structure is found at the y level of the plate center and

inward, where the collisional mean free path is 20 units or longer (much longer in the innermost layer). We assert that the gas *cannot* show meaningful structure on scales much smaller than the lesser of λ or H, and that our spatial resolution is therefore adequate for these regions. We predict, therefore, that the high-density ridges seen in Figs. 6 and 10 (and barely discernible in Fig. 7) are probably *not* narrow shocks and very likely look much as we have depicted them.

However, the mean free path is much shorter than 20 units in the outermost y levels (particularly in the Mach 6 case). It is certainly possible that structure should develop here which is smaller than our cell sizes and is smoothed into invisibility by the coarse grid. Related to this is the fact that the collision time scale in these cells is much shorter than our computational time steps, so most particles near the outer boundary can be expected to experience several collisions per time step. These will completely randomize and isotropize particle velocity dispersions while preserving the mass, momentum, and energy of each cell as a whole. But this is just the effect we expect in this short-λ, near-continuum regime, so the high collision rate apparently introduces no new biases (as long as we are only simulating time-invariant models).

Because of the large cell sizes (compared to λ) at low y, we are not confident that [redacted] required to confirm or deny our results. Nevertheless, where we *do* see structure, at the plate level and inward, the mean free path is long enough and the collision rate small enough that we feel confident of having an accurate portrayal.

We have noted that uncertainty in our results may arise from our unrealistic boundary conditions. In particular, we speculated that the specular reflection of the lower y boundary might artificially enhance velocity and density perturbations. However, the similarity of our Case T1 to Case 2 suggests that the effects of reflection are relatively minor. A boundary which reflected like a "no-slip" surface moving with speed v_x and temperature defined by v_d might be more appropriate, but as this would only affect individual particle velocities, which are in any event almost completely randomized in the outer y levels, this further refinement would not be likely to have a significant effect on our results.

A problem common to all particle representation of gases is that estimates of density, velocity, etc., in any volume element are subject to Poisson statistics with relative error proportional to the inverse square root of particle number. Good determination of local values, therefore, demands very many model particles. Unlike deterministic particle-collision models, whose computation time goes up with the square of particle number, the Monte Carlo method described in Section II requires time linearly propertional to particle number (if the mean free path is fixed). If the system modeled is time-independent, we can get equivalent statistics (and computation time) by putting a great many particles into the system at once or integrating the effects of fewer particles over numerous time steps (the approach taken here). This is strictly true only if the number of particles is sufficient that a statistically significant number of collisions occurs in each cell during each time step. Towards the very inner parts of the computational volume, this may not be the case.

The computation time of the Monte Carlo algorithm is proportional to the collision rate per molecule, which can get uncomfortably high at the outer edge of a short scale height model. As a consequence, the Monte Carlo particle dynamics approach seems limited to regions 10 or fewer scale-heights across, inadequate to model an entire centrifuge. However, the high collision rate regime is precisely where the standard equations of hydrodynamics become appropriate, so it may be possible to write a *hybrid* computer algorithm, which uses regular hydrodynamics in high density regions and particle dynamics in lower density regions.

We have already stated our belief that our Cartesian-grid models are fair qualitative approximations of rotating systems, that the positional dependence of the scale height and "centrifugal force" are of minor importance for our assumed dimensions (width and length of 200 and 600 units, respectively, compared to an assumed circumference $2\pi r \simeq 5000$ units), and that test runs with velocity-dependent acceleration are qualitatively similar to the constant-acceleration runs detailed above. However, the fact that a centrifuge is a closed, circular system may invalidate our assumption that the incoming particle flux (at $x = 0$) is an unperturbed, exponentially declining, Maxwellian gas. If the perturbations induced by a scoop extend a full circumference downstream, it would then be "running in its own wake," and our models would not be self-consistent representations. Fortunately, it appears that, *at the height and radial location of the plate*, most of the perturbed quantities have nearly returned to their unperturbed values at the downstream end of the computational volume (compare Figs. 4 and 8 to 2, and 6 and 10 to 3). However, the inward particle flux at the innermost border has still not returned to equilibrium (Fig. 11a), and the density there is still relatively high (see especially Fig. 10, top right). These deviations, locally great but rather small compared to densities and fluxes at the *plate* (cf. Fig. 7), might propagate as far as a circumference because the gas at the inner boundary is nearly *collisionless* (e.g., for Case 3, $\lambda \simeq 1000$ units at $y = 200$). A more complete modeling of the system would be necessary to determine whether such effects are significant, either a representation of an entire circular section of a centrifuge (of limited z width), perhaps using a hybrid fluid/particle code of the type discussed above, or a more modest extension of the present Cartesian "tube" to circumferential lengths, with the addition of periodic boundary conditions.

We also speculate that model "scoops" of more realistically intricate geometries and shapes than the circular, perpendicular plate considered here may be computationally feasible and might lead to still more complex and interesting predictions.

ACKNOWLEDGMENTS

We thank an anonymous referee for his helpful suggestions toward the improvement of our presentation. This work was supported in part by the Department of Energy under Grant DE-AC05-820R20900. The early development of the computational method for application to research on galactic systems was also supported in part by the National Science Foundation under Grants AST-7909935 and AST-8204256.

REFERENCES

1. C. W. ALLEN, "Astrophysical Quantities," Sects. 52, 54, Athlone Press, London, 1973.
2. G. A. BIRD, *Phys. Fluids* **13** (1969), 2676.
3. G. A. BIRD, "Molecular Gas Dynamics," Chaps. 6, 7; Appendices *D*, *F*, *G*, *H*, Oxford Univ. Press (Clarendon), London/New York, 1976.
4. L. L. CARTER AND E. D. CASHWELL, "Particle-Transport Simulation with the Monte Carlo Method," Chapts. 2, 4, ERDA Technical Information Center, Oak Ridge, Tenn, 1975.